Avalanche Simulation with SAMOS-AT

Peter Sampl[1] and Matthias Granig[2]
[1] AVL List GmbH, Graz, Austria
[2] Stabstelle Lawinensimulation, Schwaz, Austria

ABSTRACT: The simulation software SAMOS for dry snow avalanches has been used by the Austrian Service for Torrent and Avalanche Control since 1999. The software was based on a two-dimensional, depth-averaged model with Coulombian and turbulent bottom friction for the dense flow part and on a three-dimensional mixture-model for air and ice-particles, which form the powder snow part. The mixture model involved separate mass-balances for the air and ice-particles and one single balance for the momentum. Additional balances for the turbulent energy and dissipation rate were considered. The amount of powder snow generated from the dense flowing snow was predicted assuming an analogy of momentum- and mass-transfer above the dense-flow-surface. A triangular grid, moving with the flowing mass over the terrain surface, was used for the numerical solution of the dense-flow equations in Lagrangean formulation, while a three-dimensional, non-moving (Eulerian) grid, adapted to the terrain surface, was employed to solve the equations for the air-and-ice mixture. An improved version, SAMOS-AT, has been completed in 2007. The dense flow friction model was changed, so that the turbulent friction part depends also on the flow-depth. The mixture-model for the powder snow part was replaced by a full two-phase-model for air and ice-particles, with separate mass and momentum balances. A smoothed-particle hydrodynamics method is used now to solve the dense-flow-equations. The improved model is described in this paper.

KEYWORDS: Avalanche dynamics, simulation, dense flow avalanches, powder avalanches.

1 INTRODUCTION

SAMOS is a simulation-software for dry snow avalanches. It describes both the dense-flow-layer (DFL) and the powder-snow-layer (PSL) of an avalanche, as well as the interaction between them. The software has been developed for the Austrian Service for Torrent and Avalanche Control (WLV), which has used a first version since 1999 (Zwinger et al., 2003; Sampl and Zwinger, 2004). The use of the software revealed several problems: too large DFL-width in channelled terrain and often too large run-out distances of the DFL and also the PSL in terms of the 5 kPa zone. An improved version, SAMOS-AT, has been developed and completed in 2007. The main changes are different bottom friction models for the DFL, the treatment of the PSL as two-phase-flow and a different numerical solution scheme for the DFL. Furthermore, the usage of the software has been substantially simplified.

2 SAMOS-AT AVALANCHE MODEL

In SAMOS, dry snow avalanches are thought to consist of air and ice particles in variable concentrations. With the volume-fraction c and intrinsic density ρ_{ice} of the ice particles and the air density ρ_{air}, the mixture density ρ is given by

$$\rho = c\rho_{ice} + (1-c)\rho_{air} . \quad (1)$$

A vertical three-layer-structure (Figure 1) is assumed in the avalanche, the layers being identified by different ranges of the mixture density: a dense flow layer (DFL) with 200 to 300 kg·m^{-3} at the bottom, a powder snow layer (PSL) with 1 to 10 kg·m^{-3} at the top and a transition layer in between.

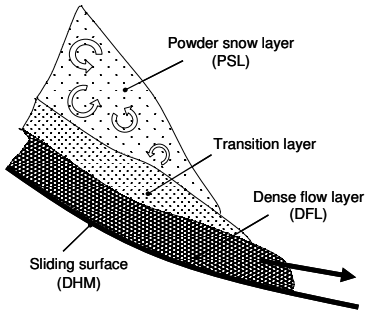

Figure 1. Vertical layer-structure of a dry snow avalanche as assumed in the SAMOS-AT model.

The transition layer and the PSL are assumed to develop above the DFL with time, depending on the flow conditions. The transition layer is not spatially resolved in the model, but reduced to an interface which connects DFL and PSL. The DFL is modelled as shallow flow in two dimensions on the terrain surface (prescribed by a digital height model (DHM)), while

Corresponding author address: Peter Sampl, AVL List GmbH, Hans-List-Platz 1, 8020 Graz, Austria;
tel: +43 316 787 439; fax: +43 316 787 1923;
email: peter.sampl@avl.com

the PSL is modelled as three-dimensional flow above the DFL, including the air masses a few hundred meters above ground.

2.1 Dense Flow Layer (DFL) Model

The DFL model is obtained by dividing the DFL into a large number of small mass elements and writing the integral mass- and momentum-balances for each of it. Each element contains a mass m_e, touches the bottom surface at an area A_e and extends up to the DFL surface. The balances result in a set of ordinary differential equations, which are coupled by the lateral forces between the elements. The DFL is assumed to be shallow: the ratio of the characteristic DFL depth H (normal to the terrain) to the DFL length (and width) L is taken to be small. All terms of order $(H/L)^{1.5}$ or smaller are neglected (following the work of Savage and Hutter, 1989; derivation see Zwinger et al., 2003). A constant bulk density ρ is assumed for the entire DFL. A smoothed-particle hydrodynamics (SPH) method (Monaghan, 1988) is used, so that the flow depth h at each point $\vec{x}$ on the terrain surface is expressed as weighted sum over all element with centers at position $\vec{x}_e$:

$$h(\vec{x}) = \frac{1}{\rho}\sum_e m_e W(\vec{x},\vec{x}_e) \qquad (2)$$

The SPH-kernel function $W(\vec{x},\vec{x}_e)$ (see 3.1) has a dimension of m^{-2}. The bottom area A_e of an element follows as

$$A_e = \frac{m_e}{\rho h(\vec{x}_e)} \qquad (3)$$

The mass and momentum balances for each element are formulated in a local coordinate system with direction 1 along the elements current flow direction $\vec{u}$ (defined as average velocity in the element), direction 3 normal to the terrain and direction 2 normal to both. For brevity, the element indices e are dropped below.

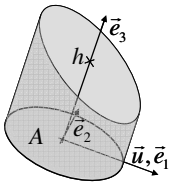

Figure 2. A DFL mass element with bottom surface A, average depth h and average velocity $\vec{u}$ and the local coordinate system $\vec{e}_1,\vec{e}_2,\vec{e}_3$.

Snow entrainment is considered at the DFL front and specified by q_{ent}, the entrainable mass per unit surface area. The front width w_f within an element, measured normal to the flow direction, is zero for elements not at the front. If the mass transferred to the PSL per unit surface area is termed j_s and the time t, the mass balance for an element can be written as

$$\frac{dm}{dt} = w_f q_{ent}\|\vec{u}\| - j_s A\,. \qquad (4)$$

The momentum balance in direction 3 yields an equation for the bottom pressure in the element

$$p^{(b)} = -(g_3 - \kappa_1\|\vec{u}\|^2)\frac{m}{A} \qquad (5)$$

with g_i the vector of gravitational acceleration and κ_1 the terrain curvature in flow direction. The momentum balances for directions i =1,2 can be written

$$\frac{d(mu_i)}{dt} = mg_i - A\frac{\partial}{\partial x_i}\left(K_{(i)}\frac{p^{(b)}}{2}h\right) - A\tau^{(b)}\frac{u_i}{\|\vec{u}\|} + F_i^{(res)} \qquad (6)$$

with $\tau^{(b)}$ the bottom shear stress and $F_i^{(res)}$ the resistance force resulting from obstacles (an additional resistance force to break entrained snow from the ground can be considered optionally; see Sailer et al, 2008). The second term on the right hand side describes the force resulting from the lateral normal stresses, which are expressed as product of the bottom pressure with the normal stress coefficients $K_{(i)}$. A linear drop of the stresses from the bottom to zero at the DFL surface is assumed, hence the average over the depth is half the bottom value. The shallowness assumption allows to neglect lateral shear stresses. The resistance force due to obstacles like trees in a forest or fields of boulders, defined by a characteristic obstacle height h_{res}, diameter d_{res}, average lateral distance s_{res} and shape resistance coefficient c_w is computed as

$$F_i^{(res)} = -c_w\rho\frac{\|\vec{u}\|^2}{2}d_{res}\min(h,h_{res})\frac{A}{s_{res}^{\,2}}\frac{u_i}{\|\vec{u}\|} \qquad (7)$$

For a granular material with internal Mohr-Coulombian friction, as assumed in SAMOS, the coefficients $K_{(i)}$ depend on the flow state and the friction parameters (Zwinger et al., 2003). The normal stress is larger than $p^{(b)}$, if the material is compressed, and smaller, if it expands. This results in a net energy loss in each compression-expansion cycle. In practice, this led to a considerable reduction of runout-distances in SAMOS when finer DHMs were used, since these resolve more surface-ripples, each causing a compression-expansion-cycle. Hence $K_{(i)} \equiv 1$ is assumed in SAMOS-AT, as for a Newtonian fluid, and the retarding effect of ripples is considered in the bottom friction parameters.

The bottom friction in SAMOS-AT is computed as

$$\tau^{(b)} = \tau_0 + p^{(b)}\mu\left(1+\frac{R_{s0}}{R_{s0}+R_s}\right)+\frac{\rho\|\vec{u}\|^2}{\left(\frac{1}{\kappa_D}\ln\frac{h}{R_D}+B_D\right)^2} \quad (8)$$

In the above relation, τ_0 is a yield stress (which is applied in small-avalanche-simulations only; see Sailer et al., 2008), μ is the Coulombian bed friction coefficient, R_s a "fluidization factor", R_D the surface roughness, and R_{s0}, κ_D and B_D empirical constants. The values used for μ, R_{s0}, κ_D, R_D and B_D are 0.155, 0.222, 0.43, 0.1 m, and 4.13, respectively.

The fluidization factor R_s is defined as the ratio of dispersive stresses to the effective bottom pressure:

$$R_s = \frac{\rho\|\vec{u}\|^2}{p^{(b)}} \quad (9)$$

The R_s-term serves to increase the Coulombian bed friction at low fluidization, so as to stop slow avalanche parts already in terrain steeper than $\mathrm{atan}(\mu)$ and to prevent spreading when mass is close to stopping.

The last term on the right hand side in (8) is inferred from classical boundary layer theory for turbulent fluid flow and the logarithmic law-of-the-wall for rough plates (see e.g. in Gersten and Herwig, 1992). These laws may be obtained by assuming turbulent eddies (i.e. larger clusters of non-coherent ice particles, or coherent snow clods), whose size is proportional to the distance from the terrain surface. The difference to the turbulent friction term as in the classical Voellmy model is the (moderate) reduction of friction with increasing flow depth h.

2.2 Transition Layer Model

The transition layer is dominated by saltation, particle-collisions, sedimentation and turbulent suspension due to the aerodynamic forces acting onto the particles at the DFL surface. The interaction of particle-suspension and the turbulence in the air is intense and complex. A strongly simplified model thus has been developed for the initial version of SAMOS and has been kept with a few modifications.

The DFL surface with the transition layer is considered to be a "rough wall" for the PSL (this wall is of course moving with the DFL-speed). With Δu the magnitude of the velocity difference between the DFL surface and the PSL at a reference height y above, equal to the assumed transition layer depth, the wall shear stress in turbulent flows at rough walls is, again from classical boundary layer theory, given by

$$\tau_w = \frac{\rho_{air}\Delta u^2}{\left(\frac{1}{\kappa}\ln\frac{y}{R_P}+B_P\right)} \quad (10)$$

R_p is the roughness length and κ (again 0.43) and B_p (8.5) constants. The suspension mass flux per DFL surface unit j_s is assumed to be proportional to the momentum flux, which is equal to τ_w. Since τ_w is proportional to Δu and j_s is to the particle concentration difference Δc, between DFL and PSL at y, the mass flux is rescaled accordingly and computed as

$$j_s = -\tau_w\frac{\Delta c}{\Delta u}\left(\frac{c_{susp}c_d}{d_p}\right) \quad (11)$$

The correction term in brackets is introduced to account for dissimilarities between momentum and particle transport. It shall reflect that particles with larger diameter d_p and smaller form-drag-coefficient c_d are transported to a lesser extent. c_{susp} is an empirical correction constant with the dimension of a length. No size distribution is considered for the particle diameter in the model. The roughness seen by the PSL is computed as

$$R_P = R_0 + c_{salt}\frac{\|\vec{u}\|^2}{|g_3|}+c_{res}\frac{\tau_w}{\rho_{ice}|g_3|} \quad (12)$$

where R_0 is the geometric roughness of the DFL surface without saltation. The second term models the increase of roughness due to saltation (with empirical constant c_{salt}) and the third the increase due to the suspended particles themselves (with yet another empirical constant c_{res}). Furthermore, it is assumed that suspension starts only at a critical saltation height of the particles at the DFL surface. The saltation height, relative to the particle diameter, is proportional to a Froude number Fr_s, computed with the DFL velocity and the condition for suspension is formulated as

$$Fr_s = \frac{\|\vec{u}\|^2}{g_3 d_p} > Fr_{s,crit} \quad (13)$$

This condition blocks suspension specifically when the DFL comes to rest. Values typically used for c_{susp}, c_d, $Fr_{s,crit}$, R_0, c_{salt} and c_{res} are 0.01, 3, 400, 0.1 m, 10^{-4} and 10, respectively. The particle diameter d_p is assumed in the range 0.5 to 1 mm.

2.3 Powder Snow Layer (PSL) Model

The PSL model in SAMOS-AT treats air and ice particles as separate phases, i.e. separate velocities are computed for both (in contrast to

the initial SAMOS version, which assumed zero slip velocity). The two phase approach allows for sedimentation of the particles and a separation of particle trajectories and air-streamlines, which may be significant in highly curved terrain.

The well known Navier-Stokes equations with turbulence-averaging are solved to compute the flow of the air phase. The compressibility of air is considered via the ideal-gas-law

$$p = \rho R_{air} T \tag{14}$$

with the static air pressure p, the air temperature T , which is assumed to be constant constant (273 K), and R_{air} the specific gas constant of air. In the following equations, all variables refer to the air, if not indicated otherwise, and all dependent variables are turbulence-averaged. The volume of the ice particles is ignored due to their small volume fraction. A global, static (Eulerian) coordinate system (coordinates x_i) with directions i =1,2,3 is used and Einsteins summation convention applies to the equations below. The air mass balance reads

$$\frac{\partial \rho}{\partial t} + \frac{\partial (\rho u_i)}{\partial x_i} = 0 \tag{15}$$

The momentum balance considers the particle drag f_i and the drag $f_i^{(res)}$ resulting from obstacles not representable via the geometric boundary conditions (e.g. forest):

$$\begin{aligned} \frac{\partial (\rho u_i)}{\partial t} + \frac{\partial (\rho u_i u_j)}{\partial x_j} &= \rho g_i - \frac{\partial p}{\partial x_i} \\ + \frac{\partial}{\partial x_j} \eta_{eff} \left(\frac{\partial u_i}{\partial x_j} + \frac{\partial u_j}{\partial x_i} \right) &+ f_i + f_i^{(res)} \end{aligned} \tag{16}$$

The effective viscosity η_{eff} consists of the laminar viscosity η_{lam} and the apparent turbulent viscosity, resulting from turbulent mixing. The widely used k-ε turbulence model (Launder et al., 1972) is employed to capture the turbulent flow effects. It requires the solution of additional transport equations for the turbulent fluctuation energy k and the turbulent dissipation rate ε. For brevity, these equations are not reproduced here. Turbulence generation and dissipation due to the particles are assumed to cancel. With the k-ε-model constant C_μ (0.09), the effective viscosity reads

$$\eta_{eff} = \eta_{lam} + \rho C_\mu \frac{k^2}{\varepsilon} \tag{17}$$

The resistance force per volume due to forest is written analogously to (7) as

$$f_i^{(res)} = \frac{d_{res}}{s_{res}} c_w \frac{\rho \|\vec{u}\|^2}{2} \frac{u_i}{\|\vec{u}\|} \tag{18}$$

The particles are treated as separate rigid bodies. The drag force exerted by the surrounding air onto a particle is formulated as (suffix p indicates particle values)

$$F_{p,i} = c_d \frac{\rho \|\Delta \vec{u}_p\|^2}{2} \frac{{d_p}^2 \pi}{4} \frac{\Delta u_{p,i}}{\|\Delta \vec{u}_p\|} \tag{19}$$

with the drag coefficient c_d and the particle diameter d_p , introduced in 2.2. The slip velocity

$$\Delta u_{p,i} = (u_i + u_i') - u_{p,i} \tag{20}$$

must consider the turbulent fluctuation part u'_i of the air velocity at the particle position. With the k-ε–model, a fluctuation velocity can be determined stochastically by picking a random vector according to a Gaussian distribution with mean value zero and a standard deviation of the vector magnitude of

$$\|u_i'\|^2 = \frac{2}{3} k \tag{21}$$

The same random velocity is kept as long as the particle travels with the same turbulent eddy, which is of size L_{turb} and has a life time t_{turb}, determined from k and ε. This time interval t_t ends when either the eddy decays or it is traversed.

$$\begin{aligned} L_{turb} &= {C_\mu}^{0.75} \frac{k^{1.5}}{\varepsilon} \quad t_{turb} = \frac{k}{\varepsilon} \\ t_t &= \min \left(\frac{L_{turb}}{\|\Delta \vec{u}_p\|}, t_{turb} \right) \end{aligned} \tag{22}$$

The particle drag force in (16) hence can be formulated as limit of a sum over all particles within a volume ΔV around the considered position

$$f_i = -\lim_{\Delta V \to 0} \frac{1}{\Delta V} \sum_p^{\Delta V} F_{p,i} \tag{23}$$

and the momentum balance for a particle with mass $m_p = \rho_{ice} {d_p}^3 \pi / 6$ reads

$$m_p \frac{du_{p,i}}{dt} = F_{p,i} + m_p g_i \tag{24}$$

Particles that hit obstacles are removed. The hit-probability within a time interval Δt is

$$P_{hit} = 1 - \left(1 - \frac{d_{res}}{s_{res}} \right)^{\frac{\|\vec{u}_p\| \Delta t}{s_{res}}} \tag{25}$$

A particle is removed, if a random number in the range [0,1), queried each time interval Δt, is smaller than P_{hit}. When a particle hits the DFL surface, it is always reflected. If it hits the terrain, it is reflected only if the velocity is larger than a threshold (of 3 ms^{-1}) and the angle be-

tween its velocity vector and the surface normal is smaller than 30°. Otherwise it is deposited.

3 NUMERICAL METHODS

3.1 DFL Numerics

The DFL momentum equation (6) is solved for a large number of mass elements (typically about 2000 kg each) explicitly in time (usually steps of 0.1 s). A regular DHM grid with a resolution of typically 5 m is used to represent the terrain and to define the SPH-kernel-function W in (2).

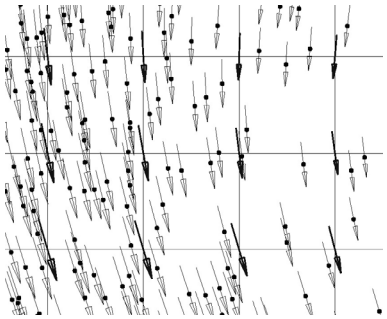

Figure 3. DHM-grid (detail), seen from above, mass element centers (dots), element velocities (light vectors) and smoothed velocity field at grid points (bold vectors).

To obtain W, a bilinear interpolation is applied first to distribute element values to the nodes of the grid cells containing the element-centers, and the same bilinear interpolation is used afterwards to get a smoothed value at the element center from the values at the surrounding grid nodes. SPH methods have the advantage of small numerical diffusion, while they may show stability problems due to the forces between the elements. In the DFL the latter are small (of order H/L), however. Furthermore, an artificial viscosity is applied to the difference between element velocity and the smoothed velocity at the element center.

3.2 PSL Numerics

A fully implicit Finite Volume method is used to solve the balances of the air flow in a SIMPLE scheme (Patankar, 1990; for implementation details, see FIRE Manual, 2009). The momentum balances for the ice-particles are integrated explicitly in time. Of course, not all particles can be followed separately. Instead, they are grouped in parcels (of about 100 kg each) and the equations are solved for one exemplaric particle in each parcel. The numerical PSL-mesh is created by extruding a regular grid (resolution typically 15 m) in direction of the average terrain normal. About 20 cell layers with increasing depth are added, with the depth of the first approximately 4 m.

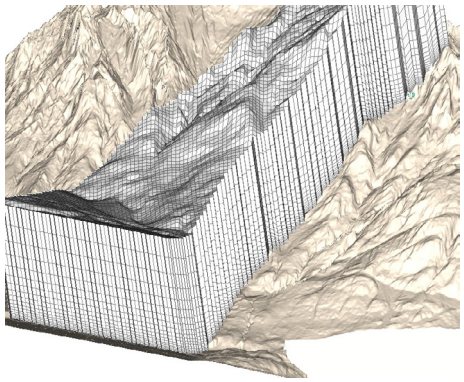

Figure 4. 3D-grid for simulation of PSL adapted to the terrain surface.

4 APPLICATION RESULTS

Model validation, application and comparisons to the initial SAMOS version are described in a separate article (Granig et al., 2009).

5 REFERENCES

FIRE CFD Solver Manual v2009, 2009. AVL List GmbH, Graz.

Gersten, K. and Herwig, H. 1992. Strömungsmechanik, Vieweg, Braunschweig, Wiesbaden.

Granig, M., Sampl, P., Tollinger, C., Jörg, Ph., 2009. Experiences in avalanche assessment with the powder snow avalanche model SamosAT. Accepted for the International Snow Science Workshop 2009, Davos, Switzerland.

Launder, B.E. and Spalding, D.B., 1972. Mathematical models of turbulence. Academic Press, London.

Monaghan, J.J., 1988. An introduction to SPH. Computer Physics Communications, vol. 48, pp. 88-96.

Patankar, S.V., 1980. Numerical heat transfer and fluid flow. McGraw-Hill, New York.

Sailer, R., Fellin, W., Fromm, R., et al. 2008. Snow avalanche mass-balance calculation and simulation-model. Annals of Glaciology, Volume 48, 183-192.

Sampl, P., Zwinger, T., 2004. Avalanche simulation with SAMOS. Annals of Glaciology, Volume 38, 393-398.

Savage, S.B. and Hutter, K., 1989. The motion of a finite mass of granular material down a rough incline. J. Fluid Mech. 199, 177-215.

Zwinger, T., Kluwick, A., Sampl, P., 2003. Simulation of Dry-Snow Avalanche Flow over Natural Terrain. In: Hutter, K., Kirchner, N. (Editors.), Dynamic Response of Granular and Porous Materials under Large and Catastrophic Deformations, Lecture Notes in Applied and Computational Mechanics. Volume. 11, Springer, Heidelberg, p. 161-194.